Comparison of similitude laws applied to multi-storey masonry structures with flexible diaphragms

Yohei Endo[1]*, Pere Roca[2]

1 Shinshu University, 4-17-1 Wakasato, Nagano 380-8553, Japan

2 DEC Department, Technical University of Catalonia (UPC-Barcelona Tech), Jordi Girona 1-3, 08034 Barcelona, Spain

* Corresponding author (endii@shinshu-u.ac.jp

Comparison of similitude laws applied to multi-storey masonry structures with flexible diaphragms

The present paper discusses similitude laws employed for the shaking-table tests of masonry structures with flexible diaphragms. Two tasks are tackled. First, the paper presents a literature review on similitude laws. The discussion focuses on Cauchy and Cauchy-Froude laws. Second, numerical analysis is performed to examine the accuracy and adequacy of the aforementioned two laws. Two previously performed shaking-table tests are taken advantage of as the case studies. The paper explores the ideal applications of similitude laws to the shaking table tests of masonry structures with flexible diaphragms by comparing the behaviour between full-scale prototypes and reduced-scale models.

KEYWORD: shaking table test, similitude law, masonry, numerical analysis, seismic assessment

1. INTRODUCTION

The paper discusses similitude laws applicable to the shaking table tests of reduced-scale models describing masonry structures. Masonry structures are considered seismically vulnerable due to the presence of flexible diaphragms and the lack of sufficiently efficient connections between orthogonal walls and between floor/roof slabs and walls (Mendes et al. 2014, Magnes et al. 2010, Gregory et al 2004). The lack of so-called box behaviour causes walls to behave independently and hinders a globally efficient response (Stavridis et al. 2016, Binda and Saisi 2005, D'Ayala and Speranza 2003). Earthquake damage surveys have indicated that such structures were particularly vulnerable in out-of-plane movement (Weise et al. 2018, Gautam 2017) although they were unignorably vulnerable also in in-plane movement (Modena et al. 2011).

Shaking table tests have been considered as an appropriate approach to closely investigate the seismic behaviour of structures. However, reliable shaking table tests are very expensive (Harris and Sabnis 1999). In some cases, specimens have to be reduced

in scale due to the capacity and size of shaking tables (Tomazevic and Velechovsky 1992). Different approaches have been taken to carry out the qualitative and quantitative comparison of seismic behaviour among full-scale prototypes and reduced-scale models (Coutinho et al. 2016). A frequently used one is similitude laws (Szirtes 2007). A number of shaking table tests have been performed on reduced-scale masonry structures with flexible diaphragms according to similitude laws. Tests were performed successfully on single-storey masonry buildings (Okail et al. 2011, Rafi et al. 2018 Kallioras et al. 2018, 2020, Paquette and Bruneau 2003, Paquette et al. 2004) and multi-storey masonry buildings (Mendes et al. 2014, Deng et al. 2019, Mouzakis et al. 2018, Senaldi et al. 2020, Sweeney et al. 2004, 2005). The size effect of units can be unignorable when the scale of masonry structures are significantly reduced (Petry and Beyer 2014a-b, Mohammed and Hughes 2011). Section 2 discusses the applications of similitude laws to shaking-table tests on reduced-scale masonry structures.

The present research discusses scale factors due to similitude laws for the shaking table tests of masonry buildings with flexible diaphragms. Two tasks are tackled. The first task is a literature review on similitude laws and on the shaking table tests of reduced-scale models. The review introduces a set of scale reduction methods including the Cauchy and Cauchy-Froude laws. Both laws are frequently used in engineering fields. Then, discussion is made on challenges to appropriately apply the two laws to masonry structures. The second task deals with pushover and nonlinear dynamic analysis (NDA) applied to full-scale prototypes and reduced-scale mock-ups by numerical simulation. Two previously conducted shaking table tests are taken advantage of as the case studies. The mock-ups are scaled according to Cauchy or Cauchy-Froude law. In the application of Cauchy law, the gravity value is kept original (i.e. 9.81 m/s^2). Comparing behaviour between the porotypes and mock-ups, the advantages and limitations of the two laws are

investigated and discussed. The influences of input signals on the behaviour of reduced-scale models are also examined by considering two types of accelerograms. One is generated from code-based spectra while the other from real earthquakes. Although a variety of shaking table tests have been performed on reduced-scale mock-ups, the accuracy of similitude laws has not been fully examined, referring to the comparison of nonlinear behaviour between prototypes and mock-ups. The paper suggests the appropriate choices and applications of similitude laws for the shaking–table tests of masonry buildings with flexible diaphragms.

2. DISCUSSION ON SIMILITUDE LAWS

2.1 Overview of similitude laws

In engineering fields, it is not exceptional to perform experiments using scaled models due to the high cost of full-scale models and limitations related to the capacity of actuators (Coutinho et al. 2016). There are different approaches to correlate the behaviour between full-scale prototypes and reduced-scale mock-ups including dimensional analysis, energy methods, similitude laws and empirical similarity methods (Casaburo et al. 2019). Similitude laws have been one of the major approaches (Szirtes 2007). An advantage of them lies in governing equations. The equations fix a set of conditions and permit the clear correlations of variables between the full-scale prototypes and mock-ups (Casaburo et al. 2019). It is said that Kline (1965) was the first scholar who presented comprehensive discussion on similitude laws. Krawinkler (1979) presented a pioneering work on similitude laws in structural engineering. In his paper, an artificial mass simulation law (AMS) was proposed. AMS applies additional masses to models to obtain the same horizontal and shear stress as in prototypes under seismic

loadings. Harris and Sabnis (1999) presented an extensive review on similitude laws applicable to the dynamic testing of masonry structures.

2.2 Application of similitude laws to masonry structures with flexible diaphragms

Among a variety of similitude laws, Cauchy law (C law) and Cauchy-Froude law (CF law) have been frequently used for the shaking table tests of masonry structures (Carvalho 1999, Harris and Sabnis 1999, Szirtes 2007, Coutinho et al. 2016). Table 1 introduces some of well-known and recently proposed similitude laws including C law and CF law. In the table, the scale factor λ denotes the length scale; the prototype length is divided by the mock-up length. C law is effective when tests focus on restoring forces that are based on stress-strain constitutive relationships (Carvalho 1999). As an advantage, C law does not require the modification of material properties including the mass density of the materials. On the other hand, it needs to increase the acceleration by λ times. Thus, in order for a test to follow C law precisely, gravity needs to be increased as well. However, it is almost impossible to modify gravity in typical laboratory facilities. Some tests were performed, ignoring a relationship between inertial force and gravity force (Avila et al. 2012, Mendes et al. 2014, Deng et al 2019). Such an approach can be effective when the vertical compressive stress has little influence on lateral stiffness (Krawinkler 1979). Under CF law, the combination of C law and Froude law, the acceleration of mock-ups is equal to prototypes. In contrast, the density of materials needs to be controlled so that the mock-ups reproduce the same working stress state in the walls as the prototypes under CF law. Since this is not easily fulfilled, an adjustment is made. It can be done by controlling the strength of materials (Jurukovski et al. 1992, Tomazevic and Velechovsky 1992, Zarnic et al. 2001), placing additional masses (Tomazevic et al. 2009, Benedetti et al. 1998, Dolce et al. 2005, Vintzileou et al. 2015,

Beyer et al. 2015) or alternatively prestressing walls/columns (Zonta et al. 2001, Hashemi and Mosalam 2006, Rafi et al. 2018). Tests may be performed by implementing the combinations of the above-mentioned approaches (Tomazevic and Velechovsky 1992, Bothara et al. 2010). The locations of additional masses are highly influential in dynamic behaviour (Krawinkler 1979, Tomazevic and Velechovsky 1992). When additional masses are incorrectly located, mock-ups may show higher capacity than prototypes (Benedetti et al. 1998). In addition, flexible floor slabs may transfer the loads from the masses mainly to the walls which timber joists rest on (Bothara et al. 2010, Vintzileou et al. 2015). An intermediate solution between C law and CF law may be used (Carvalho 1999). In this case, the scale factor of each parameter is determined, based on aspects such as the responses of mock-ups, the capacity of shaking tables and so on (Deng et al. 2019, Senaldi et al. 2020 see Table 1).

3. RESEARCH METHODOLOGIES

The paper compares C law and CF law applied to masonry structures with flexible diaphragms. The two laws are chosen in this paper as they have been frequently used for the shaking table tests of masonry structures as discussed in Section 2.2. Structures used in previously performed shaking-table tests are considered as the case studies for the present research. The descriptions of the structures are found in Section 4 and Section 5. Three types of models are prepared. The first model represents the full-scale prototype (named prototype in this paper). The second one is scaled according to CF law (mock-up CF). The third is according to C law (mock-up C). The adopted CF law assumed that additional masses are distributed over the masonry walls by increasing the density of the masonry. In the adopted C law, gravity acceleration remains unchanged, as it represents a typical condition of shaking-table facilities. It is called

simplified C law in the paper. The strength of the masonry is not modified in the application of both laws.

Pushover analysis and NDA are performed. As for pushover analysis, incremental forces are applied, according to the mass distributions of the structures. As for NDA, two input signals are considered to examine their influences on structures. One is generated from a real earthquake. The Kalamata earthquake (named KMT in this paper) is considered in this study. The accelerograms are taken from the website of Engineering Strong Motion Database (Luzi et al. 2016). It occurred at 17:24 (local time) on September 13, 1986 in Greece. The magnitude was 5.9 (Mw) and 5.5 (M_L), respectively. The considered accelerograms were recorded at the KAL1 station. Two records (EW, NS direction) are used. The NS direction is much stronger than the EW direction in terms of the maximum spectral acceleration (Figure 1a-b). They present steep local peaks between the period range of 0.5 and 1 second (Figure 1e). The other set of accelerograms are artificial ones (ART named in this paper), generated in accordance with the European standard (CEN 2005). The spectrum type was considered type1. The ground type was A. The importance class was II. The two utilised accelerograms (ART_X, ART_Y) are almost identical (Figure 1c-d). The comparison of the spectrum shapes indicates that the two set of accelerograms (KMT, ART) are evidently different (Figure 1e). Alias intensities were 0.543 m/second and 0.737 m/second for KMT in the EW and NS directions, respectively. They were 1.767 m/second and 1.877 m/second for ART_X and ART_Y, in turn. The accelerograms were applied according to the Newmark-beta method. The constant average acceleration was used with the parameters of γ=0.5 and β=0.25. The results presented in the paper (displacement, acceleration, time, force, frequency) are normalised to those of the prototypes.

4 ANALYSIS OF A TWO-STOREY BUILDING

4.1 Description of the case study

The first case study is a half-scale two-storey stone masonry structure (Vintzileou et al. 2015). Shaking table tests were performed at the Laboratory for Earthquake Engineering/National Technical University of Athens (LEE/NTUA) in Athens, Greece. The structure was subjected to accelerograms generated from the Kalamata earthquake in the horizontal directions. The ground motions were gradually increased up to base acceleration equal to 0.24g and 0.29g in the longitudinal and transverse directions, in turn. The structure was scaled, taking into account CF law. Masonry walls were composed of three leaves. The external leaves were built of limestone units and lime mortar while the internal one was composed of limestone aggregates and lime mortar. The structure had a non-symmetric plan (Figure 2a). The dimensions were 3.65 m×2.30 m in plan (Figure 2b). The height of each floor was equal to 1.60 m and the total height of the structure was equal to 3.20 m. The walls were 0.25 m thick. The south elevation had an entrance and a window in the ground floor and two windows in the first floor. The dimensions of the entrance were 0.6 m ×1.2 m while that of the windows were 0.6 m×0.5 m. In the north elevation, two windows were positioned in each floor. A window was present in each floor of the east and west elevations. Slabs were located at the mid height and top height. 10-mm thick timber boards were laid perpendicular to timber beams and nailed to them (two nails per beam). The cross section of the timber beams was 60 mm×100 mm. They were spaced at 340 mm. The used timber was C-22 grade according to the European standard (CEN 2003).

4.2 Description of the FE model

In this study, the numerical model was composed of masonry walls, lintels over the openings and timber beams (Figure 2c). They were discretised with four-node curved shell elements. The number of nodes was 4,491 and the number of elements was 3,846. The model consisted of 3,806 four-node curved shell elements and 40 four-node line interface elements. It was fully constrained along the bottom of the walls. It is noted that the slabs were not discretised in the models. Instead, their dead weight was included by increasing the density of the timber beams. Since they were just nailed to the timber beams and sat partially on masonry walls, their structural contributions were considered of little significance.

Mechanical parameters were determined based on laboratory tests and empirical equations to estimate masonry strength (PIET 70 1971, Dayaratnam 1987, CEN 1996, Gumaste et al. 2007, Kaushik et al. 2007) (Table 2). In fact, uniaxial compression tests were performed on two masonry wallettes in advance of the shaking table test (Vintzileou et al. 2015). Compressive strength was equal to 4.33 MPa in average while modulus of elasticity equal to 0.84 GPa. The modulus of elasticity of masonry was reduced nearly by 60% in this study, compared to that which was measured by the uniaxial compression tests. It has been reported that it may be necessary for the numerical simulation of masonry structures to consider an equivalent modulus of elasticity based on the comparison of behaviour between a numerical model and the real structure (Senthivel and Lourenço 2009, Araújo 2014, Basaran et al. 2016, Maccarini et al. 2018, Howlader et al. 2020, Aşıkoğlu et al. 2020). In this paper, this decision was taken, considering the following four remarks from previous studies. First, the elastic stiffness of masonry wallettes obtained by uniaxial compression tests is often dependent on the size and bonding patterns of specimens (Lourenco 1996, Domede and Sellier

2010, Aras et al. 2011). Second, the elastic stiffness of masonry walls is subject to the thickness and strength of mortar that may not necessarily be uniform in an entire structure (Pande et al. 1989, Ma et al. 2001, Russo 2013). Third, the stiffness of masonry walls is highly influenced by the level of axial loads (Magenes and Calvi 1992, Petry and Beyer 2014b). Fourth, the macro-modelling numerical simulation of masonry structures may require adjustments to simulate properly the contributions of flexible diaphragms to masonry walls and the absence of box behaviour due to continuum and homogeneous nature (Mendes 2012, Clementi et al. 2017, Solarino et al. 2019).

Tensile fracture energy was scaled by λ times (F^*L^{-1} [N/m], see Table 1). Thus, the tensile fracture energy adopted for the prototype was equal to 30 N/m while that of the mock-up C and mock-up CF was 15 N/m. The mechanical parameters of the timber were determined considering the C-22 grade. Rayleigh damping was considered. The damping ratio was considered equal to 5%. The values of a_0 and a_1 of the prototype, mock-up CF and mock-up C were (a_0, a_1) equal to (0.5070, 0.0011), (0.7717, 0.0009) and (1.3373, 0.00054) respectively.

As for the failure criteria for masonry, the Dracker-Prager criterion in compression and the Rankin in tension were considered. For timber, the Von Mises criterion was adopted both in compression and in tension. The Mohr-Coulomb frictional behaviour was adopted for connections between timber beams and masonry walls. Frictional values were determined, taking into account typical frictional behaviour between masonry with lime mortar and timber (Vintzileou 2008, Moreira et al. 2014). The friction angle was 26.6^o ($\tan\Phi$=0.5). Normal linear stiffness was 100 kN/mm^2 and shear linear stiffness was 50 kN/mm^2. Cohesion was 0.2 MPa. As for the mock-up CF, additional masses equal to 12.8 tons were distributed uniformly over the walls. It is noted that the mass

distribution patterns of the mock-up CF were not the same as the performed shaking table test. In the test, due to the capacity of the shaking table, it was not possible for the additional masses to be placed according to CF law.

4.3 Eigenvalue analysis

Eigenvalue analysis was carried out to compare behaviour between the prototype, mock-up C and mock-up CF. Table 3 compares the eigenvalues and participation factors (PFs) of the first and second mode. The eigenvalues and mode shapes of each mode were almost identical (Figure 3). As an additional case, eigenvalue comparison was made between the FE model and real structure. In this case, the additional masses were located in the same patterns as in the shaking table test. In total, masses amounting to 8 tons were used: 4.5 tons over the mid slab and 3.5 tons over the top slab. The eigenvalues showed good agreement with the real structure with error less than 2% (Table 4).

4.4 Nonlinear static analyses

Pushover analysis was carried out in the X and Y directions. In both positive and negative X directions, the initial stiffness was equal in the three models (Figure 4a, Figure5a). The prototype and mock-up CF showed very similar base acceleration-displacement (a-δ) relations although the mock-up C ended in lower acceleration and higher ductility than the prototype. Comparable damage patterns were seen in the three models although damage intensities were slightly different. It is noted that a red circle in a figure indicates an area in which the largest principal strains are found in a structure. Damage was seen around the openings of the north and south walls due to in-plane movement both in the positive and negative X directions (Figure 4b-d, Figure 5b-d).

The mock-up C presented more extensive damage around openings of the first floor than the other two models.

The initial stiffness was equal in the three models in the positive and negative Y directions (Figure 6a). In the positive Y direction, the prototype (0.263g, 20.7 mm) and mock-up CF (0.265g, 20.6 mm) showed close maximum base acceleration and displacement at the top height. In contrast, the mock-up C showed 8.6% lower base acceleration and 1.1% higher displacement than the prototype (0.241g, 21.0 mm). In the negative Y direction, the prototype and mock-up CF also showed close maximum response values while the mock-up C presented about 3.6% lower base acceleration and displacement than the prototype. The three models showed indistinguishable damage patterns. In the positive Y directions, damage was seen around the openings of the longitudinal walls of the ground floor (Figure 6b-d). In the negative Y direction, damage was observed around the openings of the longitudinal walls of the ground and first floors (Figure 7b-d). The mock-up CF showed closer maximum response values to the prototype than the mock-up C although the three models showed similar damage patterns. It is noted that the mock-up C showed severer damage than the prototype and mock-up CF especially in the X directions.

An additional case was analysed, considering a different condition of C law. Gravity was increased by λ times according to the length scale of the model. It is called exact C law in this paper as opposed to the simplified C law. The model is named the mock-up eC. As expected, in both X and Y directions, the mock-up eC showed much more similar results to the prototype than the mock-up C in terms of the a-δ relation and damage patterns (Figure 4-7e).

4.5 Nonlinear dynamic analysis

As discussed in Section 3, two sets of accelerograms were applied and compared. The accelerograms in the X and Y directions were applied at the same time. Time intervals were equal to 0.000666 seconds. As for KMT, the accelerogram of the EW direction was applied in the X direction while that of the NS direction was applied in the Y direction. The time history of displacement was almost identical in the three models (Figure 8a). The a-δ relations of the three models showed similar plots (Figure 8b). In the prototype and mock-up CF, the north and south walls showed damage around the top of the mid span (Figure 8c-d). Damage was caused principally by their out-of-plane movement but diagonal damage running from an opening suggests that in-plane movement was also relevant (Figure 8c-d). The west wall presented vertical damage around the top-corner due to the out-of-plane movement of the south wall. In the mock-up C, the north and south walls showed extensive damage around openings due to their in-plane movement (Figure 8e). In addition, the west wall presented damage running diagonally from an opening due to its in-plane movement.

As for ART, ART_X was applied in the X direction while ART_Y in the Y direction. The displacement time-history at the top of the structure showed almost identical in the three models (Figure 9a). The a-δ relations showed similar shapes between the models (Figure 9b). The three models presented damage in similar locations of each wall mainly due to the out-of-plane movement of the north and south walls (Figure 9c-e). The north and south walls showed damage around the top of the mid-span. The east and west walls showed vertical damage in top corners. However, the mock-up C and mock-up CF presented damage running diagonally in the top-middle of the north and south walls (Figure 9d-e). The north and south walls of the mock-ups exhibited damage due to the combination of the in-plane and out-of-plane movement of them (Figure 9d-e).

Under KMT, the mock-up C presented severe damage patterns including in-plane damage in the north and south walls. Apart from it, the three models showed damage in similar locations. Under ART, they showed comparable damage patterns mainly due to the out-of-plane movement of the north and south walls. The a-δ relations were very similar as well.

5 ANALYSIS OF A FOUR-STOREY BUILDING

5.1 Description of the case study

The second case-study is a one-third scale four-storey stone masonry structure (Mendes et al. 2014) (Figure 10a). The structure was tested, using a shaking table at the National Laboratory for Civil Engineering (LNEC) in Lisbon, Portugal. A series of input signals was applied with intensity increased up to 0.469g and 0.461g in the longitudinal and transverse directions, in turn. As input signals, artificial accelerograms were used. They were generated, taking into account the European standard (EN1998-3). The structure was scaled according to C law. Gravity acceleration was not scaled. Masonry was composed of irregular shaped limestone units and lime mortar. Walls were composed of a single leaf. It is noted that more portions of mortar were used for the transverse walls than for the longitudinal ones, as it may have ended in different masonry strength between the orthogonal walls (Mendes 2012). The structure had a symmetric plan (Figure 10b). The dimensions were 3.15 m×4.15 m in plan. The walls were 0.17 m thick. The dimensions were 0.3 m×1.20 m. Openings were located only in the transverse walls. In each floor, four openings were present. The height of each floor was equal to 1.20 m and the total height of the specimen was equal to 4.80 m. The slabs were composed of timber beams and medium-density fibreboard (MDF) panels. The

cross section of the timber beams was 75 mm×100 mm. They were spaced at 350 mm. The MDF panels were 12 mm thick. The panels were nailed to the beams.

5.2 Description of the FE model

Masonry walls, timber beams and MDF panels were discretised in this study (Figure 10c). The number of nodes was 9,609 and the number of elements was 8,178. The masonry walls were discretised with 6,335 four-node curved shell elements. The timber beams and MDF panels were with 1,200 and 539 two-node beam elements, respectively. Interface behaviour was modelled with 80 four-node line interface elements between the beams and walls and 24 two-node point interface elements between the boards and walls. The model was fully constrained along the bottom of the walls.

The mechanical parameters of masonry and timber were chosen based on material characterisation tests (Mendes et al. 2014) and the references mentioned in Sections 4.2 (Table 5). The compressive strength and modulus of elasticity of the longitudinal walls were determined based on the uniaxial compression tests performed on wallettes composed of the same masonry as the longitudinal walls (Mendes et al. 2014). The compressive strength and modulus of elasticity of the transverse walls were determined, considering the different amounts of mortar used for the masonry walls as discussed in Section 5.1. The proportion of mortar in masonry plays a significant role in masonry strength (Valluzzi et al. 2004). It has been reported that the ratio of elastic stiffness to compressive strength may vary in the range of 300 and 800 for stone masonry, depending on masonry morphology (Van et al. 2019, Kržan et al. 2015). Tensile strength was considered to be a very low value (0.1 MPa), referring to diagonal compression tests performed on masonry wallettes (Mendes et al. 2014) and a possible

value range of traditional stone masonry (Kržan et al. 2015, Tomachevic 1999). The modulus of elasticity of the MDF panels was determined, taking into account their limited contributions to the structure. Thus, they were just nailed to the timber beams. Like in the analysis performed in Section 4, the tensile fracture energy of the mock-ups was reduced by length scale (i.e. 1/3 in this case). Rayleigh damping was considered. The damping ratio was considered equal to 3%. The values of a_0 and a_1 of the prototype, the mock-up CF and mock-up C were as follows: (a_0, a_1) equal to (0.5070, 0.0011), (0.7717, 0.0009), (1.3373, 0.00054), respectively.

The same approach as discussed in Section 4.2 was taken for failure criteria. For masonry, the Dracker-Prager in compression and the Rankin in tension were adopted. For timber, the Von Mises model was adopted both in compression and in tension. The Mohr-Coulomb frictional behaviour was adopted to the connections between the timber beams and longitudinal walls and those between the timber slabs and transverse walls. The friction angle was 26.6° ($\tan\Phi$=0.5). Normal linear stiffness was 100 kN/mm^2 and shear linear stiffness was 50 kN/mm^2. Cohesion was 0.2 MPa. As for the mock-up CF, masses equal to 43.8 tons were uniformly distributed over the walls.

5.3 Eigenvalue analysis

Table 6 compares eigenvalues and PFs between the prototype, mock-up C, mock-up CF and the tested real structure. The eigenvalues and mode shapes of each mode were almost identical (Figure 11). The mock-up C showed close eigenvalues to those of the real structure both in X and Y direction.

5.4 Nonlinear static analysis

Nonlinear static analysis focused on behaviour in the X direction, as the structure was evidently more vulnerable in this direction than in the Y direction. Taking

advantage of the symmetry of the structure, the analysis was performed only in the positive X direction. The a-δ relations of the prototype and mock-up CF were very similar (Figure 12a). However, the mock-up C showed higher initial stiffness than the other two models and ended in the lower values of acceleration and displacement. The difference of the maximum responses was due to treatment of gravity acceleration in C law. The three models showed in-plane damage around the left side of the second- and third-floors (Figure 12b-c). In addition to it, the mock-up C exhibited damage in the right side of the second- and third-floors (Figure 12d). Like the two-storey building, another analysis was carried out on the mock-up eC. It showed very similar results to the prototype. The a-δ relations plotted exactly the same curve although the mock-up eC ended in 19.0% higher ultimate displacement values than the prototype (32.9 mm vs 27.6 mm). Damage patterns were indistinguishable (Figure 12e).

5.5 Nonlinear dynamic analysis

Two different accelerograms (KMT, ART) were adopted and compared. In both cases, the input signals were applied in horizontal directions (X and Y). Time intervals were equal to 0.0015 seconds. As for KMT, the accelerogram of the NS direction was applied in the X direction while that of the EW direction in the Y direction. The displacement time histories of the prototype and mock-up CF were almost identical but that of the mock-up C showed different values at local peaks after 1 second (Figure 13a). The a-δ relation of the mock-up C also became noticeably different from those of the other two models in the last cycle (Figure 13b). These observations may suggest that the mock-up C started to show different behaviour from the prototype and mock-up CF once damage was accumulated. The three models showed comparable damage patterns. Evident in-plane damage was observed around the left side of the second- and third-floors (Figure 13c-d). However, the mock-up C demonstrated less damage intensity than

the other two models (Figure 13e). Under ART, when displacement time histories were compared, the prototype and mock-up CF are almost equal but the mock-up C showed a different shape especially after 3.3 seconds (Figure 14a). The prototype and mock-up CF presented similar a-δ relations although that of the mock-up C was noticeably different from the other two models (Figure 14b). This may indicate that when damage levels are severe, the prototype and the mock-up may start to show different behaviour. The prototype and mock-up CF showed damage around the left side of the second- and third-floors due to in-plane movement (Figure 14c-d). The mock-up C also presented damage in the same locations as the other two models (Figure 14e). In addition, moderate in-plane damage was distributed over walls. Under both KMT and ART, the behaviour of the three models was sufficiently comparable in spite of damage intensity difference. However, the displacement time history of the mock-up C under ART was different from the other two models.

The mock-up C showed noticeably different results from the prototype especially under ART. A similar tendency was seen in the two-storey building as well. However, the difference in results was larger for the four-story building than the two story building. Since simplified C law did not scale gravity, the dead loads of the mock-up C were smaller than for the prototype by λ^3 times. In addition, the four-storey building was nearly twice as tall as the two-storey building. Such influences of difference in the dead loads and height became more evident in the four-storey building. It is added that ARTs were generated from smooth design spectra while KMTs presented local peaks and valleys in spectra (see, Figure 1e). These observations suggest that accelerogram types may need to be selected carefully especially when the dead loads and height of a mock-up are noticeably different from those of a prototype.

6 DISCUSSION

6.1 Similitude laws for shaking table tests of masonry mock-ups

Similitude laws permit qualitative and quantitative comparison of seismic behaviour between the full-scale prototypes and reduced-scale mock-ups. The use of governing equations is an advantage of the similitude laws. By means of the equations, variables are correlated between prototypes and mock-ups. C law and CF law have been frequently used for the shaking table tests of masonry structures. C law requires the modification of acceleration, as it should be applied to gravity as well. It is almost impossible to control gravity and the interpretation of results may require adjustments. CF law requires the control of material densities to reproduce the same working stress state as the prototype. It is typically done by adding masses to the structure. The locations of the masses have to be chosen carefully, as they have significant influences on dynamic behaviour. In addition, flexible diaphragms may transfer the dead loads of additional masses mainly to walls on which the beams sit, as it ends in the inaccurate simulation of the stress distributions.

6.2 Comparison between Cauchy and Cauchy-Froude laws

C law and CF law were examined by performing pushover analysis and NDA on a half-scale two-storey building and one-third scale four-storey building. Results were compared between the prototype and reduced-scale mock-ups. Regarding the pushover analysis of both buildings, the mock-up C showed more severe and distributed damage patterns than the prototype and mock-up CF while the prototype and mock-up CF presented similar damage patterns. As for the NDA of the half-scale buildings, both mock-up C and mock-up CF showed satisfactorily comparable results with the prototype. As for the NDA of the one-third scale building, when the mock-up C reached

a severe damage state, it started to show noticeably different behaviour compared to the prototype. These remarks indicated that the application of C law may need to be executed carefully when the influences of gravity are not ignorable. In fact, comparison between exact and simplified C law implied that the gravity value may have been a relevant factor for the behaviour of mock-ups. The mock-up scaled by the exact C law showed almost identical behaviour with the prototype.

6.3 Influences of accelerogram types on behaviour of masonry structures

Two types of accelerograms were considered for NDA. One was artificial accelerograms generated from code-based smooth spectra. The other was accelerograms generated from real earthquakes. Inter-storey drifts are compared between the prototype and mock-ups to examine the influences of accelerogram types on them. The half-scale two-storey building showed almost identical values both under NDA as well as pushover analysis (Figure 15). However, the one-third four-storey building exhibited noticeable differences (Figure 16). Artificial accelerograms showed the inter-storey drifts of the mock-up C were nearly in a linear shape while those of the prototype and mock-up CF were in a zigzag shape. Thus, the difference of accelerogram types was evidently seen in the upper storeys of the mock-up C of the four-storey building (see, Figure 16). It is added that the performed analyses showed that NDA under artificial accelerograms permitted a more gradual development of damage.

7 CONCLUSIONS

There is no unique answer for the best implementation of similitude laws for the tests of reduced-scale mock-ups. Similitude laws must be properly set up to execute the shaking-table tests of reduced-scale masonry structures. The paper compared the Cauchy law and Cauchy-Froude laws by means of pushover and nonlinear dynamic

analysis. Discussion focused on the comparison of damage patterns and base acceleration-displacement relations. In the elastic range, both laws showed similar behaviour among the prototype and mock-ups. Nonetheless, at a severe damage state, the mock-ups of Cauchy law of the four-storey building started to exhibit noticeably different behaviour from the prototype. This difference was attributed to the treatment of the self-weight between the mock-ups and prototype. In the performed analyses, the scaling criteria of the Cauchy law for accelerations were not applied to gravity. When the self-weight of the mock-ups has a sensible role and cannot be neglected, the Cauchy-Froude law may be appropriate in spite of the problems related to the locations of additional masses. Except for such cases, Cauchy law is considered satisfactory for masonry structures with flexible diaphragms. Not only the application of the law is straightforward but also results can be sufficiently reliable for quantitative comparison with the prototype.

The performed nonlinear dynamic analysis considered code-based artificial accelerograms and those generated from real earthquakes. The artificial accelerograms permitted the gradual development of damage as they were derived from smooth spectra without peaks and valleys. However, this implies that real accelerograms may cause a brittle collapse to the structure. Such a collapse is likely to occur to the structures of limited seismic strength. In this regard, artificial accelerograms may be preferable to real accelerograms for the shaking-table tests of masonry structures with flexible diaphragms as they permit the close observation of gradual damage evolution. However, artificial accelerograms need to be used with caution, since they may disregard the critical characteristics of target ground motions such as frequency content, soil conditions and distance from the epicentre.

Acknowledgments

This work was supported by the Japan Society for the Promotion of Science (Tokyo) under the Promotion of Joint International Research (Fostering Joint International Research (B)) (Grant number: 18KK0124).

Declaration of interest statement

No potential conflict of interest was reported by the authors.

References

References

Aşıkoğlu A, Vasconcelos G, Lourenço PB and Pantò B (2020) Pushover analysis of unreinforced irregular masonry buildings: Lessons from different modeling approaches. Engineering Structures, 218, 110830.

Aras F, Krstevska L, Altay G and Tashkov L (2011) Experimental and numerical modal analyses of a historical masonry palace. Construction and Building Materials, 25(1), 81-91.

Araújo ASFF (2014). Modelling of the seismic performance of connections and walls in ancient masonry buildings. Ph.D. dissertation, University of Minho: Portugal.

Avila L, Vasconcelos G and Lourenço PB (2012) Experimental investigation on the seismic behaviour of new concrete block masonry buildings, 15th International Brick and Block Masonry Conference, Florianópolis, Brazil, (10 pages).

Basaran H, Demir A, Ercan E, Nohutcu H, Hokelekli E and Kozanoglu C (2016) Investigation of seismic safety of a masonry minaret using its dynamic characteristics. Earthquakes and Structures, 10(3), 523-538.

Benedetti D, Carydis P and Pezzoli P (1998) Shaking table tests on 24 simple masonry buildings. *Earthquake engineering & structural dynamics*, *27*(1), 67-90.

Beyer K, Tondelli M, Petry S and Peloso S (2015) Dynamic testing of a four-storey building with reinforced concrete and unreinforced masonry walls: prediction, test results and data set. *Bulletin of Earthquake Engineering*, *13*(10), 3015-3064.

Binda L and Saisi A (2005) Research on historic structures in seismic areas in Italy. *Progress in Structural Engineering and Materials*, *7*(2), 71-85.

Bothara JK, Dhakal RP and Mander JB (2010) Seismic performance of an unreinforced masonry building: an experimental investigation. *Earthquake Engineering & Structural Dynamics*, *39*(1), 45-68.

Carvalho E (1999) Seismic testing of structures. In *Earthquake Engineering-Invited Papers: Proceedings of the eleventh European conference* (Vol. 2, p. 53).

Casaburo A, Petrone G, Franco F and De Rosa S (2019) A review of similitude methods for structural engineering. *Applied Mechanics Reviews*, *71*(3).

CEN (Comité Européen de Normalisation) (1996) Eurocode 6: Design of masonry structures Part 1-1: General rules for buildings -Reinforced and unreinforced masonry. Brussels: CEN.

CEN (2003) European Standard.EN338-2003: Structural Timber–Strength Classes; CEN: Brussels, Belgium.

CEN (2005). European Standard EN1998-3: 2005: Eurocode 8: Design of structures for earthquake resistance, Part 3: Assessment and retrofitting of buildings.

Gregory L. Cohen L, Klingner R, Hayes J, and Sweeney S (2004) Seismic evaluation of low-rise reinforced masonry buildings with flexible diaphragms: I. Seismic and quasi-static testing. Earthquake Spectra 20.3, 779-801.

Clementi F, Pierdicca A, Formisano A, Catinari F and Lenci S (2017) Numerical model upgrading of a historical masonry building damaged during the 2016 Italian earthquakes: the case study of the Podestà palace in Montelupone (Italy). Journal of Civil Structural Health Monitoring, 7(5), 703-717.

Coutinho CP, Baptista AJ and Rodrigues JD (2016) Reduced scale models based on similitude theory: A review up to 2015. *Engineering Structures*, *119*, 81-94.

D'Ayala D and Speranza E (2003) Definition of collapse mechanisms and seismic vulnerability of historic masonry buildings. *Earthquake Spectra*, *19*(3), 479-509.

Dayaratnam P (1987) Brick and reinforced brick structures New Delhi, India: Oxford and IBH

Deng M, Dong Z, Wang X, Zhang Y and Zhou T (2019) Shaking table tests of a half-scale 2-storey URM building retrofitted with a high ductility fibre reinforced concrete overlay system. *Engineering Structures*, *197*, 109424.

Dolce M, Cardone D, Ponzo FC and Valente C (2005) Shaking table tests on reinforced concrete frames without and with passive control systems. *Earthquake engineering & structural dynamics*, *34*(14), 1687-1717.

Domede N and Sellier A (2010) Experimental and numerical analysis of behaviour of old brick masonries. In Advanced materials research (Vol. 133, pp. 307-312). Trans Tech Publications Ltd.

Gautam D (2017) Seismic performance of world heritage sites in Kathmandu valley during Gorkha seismic sequence of April–May 2015. *Journal of Performance of Constructed Facilities*, *31*(5), 06017003.

Gumaste, KS, Rao KN, Reddy BV and Jagadish KS (2007) Strength and elasticity of brick masonry prisms and wallettes under compression. *Materials and structures*, *40*(2), 241-253.

Harris HG and Sabnis G (1999) *Structural modeling and experimental techniques*. CRC press.

Hashemi A and Mosalam KM (2006) Shake-table experiment on reinforced concrete structure containing masonry infill wall. *Earthquake engineering & structural dynamics*, *35*(14), 1827-1852.

Howlader MK, Masia MJ and Griffith MC (2020) Numerical analysis and parametric study of unreinforced masonry walls with arch openings under lateral in-plane loading. Engineering Structures, 208, 110337.

Jurukovski D, Krstevska L, Alessi R, Diotallevi PP, Merli M and Zarri F (1992) Shaking table tests of three four-storey brick masonry models: Original and strengthened by RC core and by RC jackets. In *Proceedings of the 10th world conference on earthquake engineering, Madrid, Spain*.

Kallioras S, Guerrini G, Tomassetti U, Marchesi B, Penna A, Graziotti F and Magenes G (2018) Experimental seismic performance of a full-scale unreinforced clay-masonry building with flexible timber diaphragms. *Engineering Structures*, *161*, 231-249.

Kallioras S, Correia AA, Graziotti F, Penna A and Magenes G (2020) Collapse shake-table testing of a clay-URM building with chimneys. *Bulletin of Earthquake Engineering*, *18*(3), 1009-1048.

Kaushik, HB, Rai DC and Jain SK (2007) Stress-strain characteristics of clay brick masonry under uniaxial compression. *Journal of materials in Civil Engineering*, *19*(9), 728-739.

Kline SJ (1965) *Similitude and approximation theory*. Springer Science & Business Media.

Krawinkler H (1979) Possibilities and limitations of scale-model testing in earthquake engineering. In *Proceedings of the second US national conference on earthquake engineering. Stanford, California* (pp. 283-292).

Kržan M, Gostič S, Cattari S and Bosiljkov V (2015) Acquiring reference parameters of masonry for the structural performance analysis of historical buildings. Bulletin of earthquake engineering, 13(1), 203-236.

Luzi L Puglia R, Russo E and ORFEUS WG5 (2016) Engineering Strong Motion Database, version 1.0. Istituto Nazionale di Geofisica e Vulcanologia, Observatories & Research Facilities for European Seismology. doi: 10.13127/ESM"

Ma G, Hao H and Lu Y (2001) Homogenization of masonry using numerical simulations. Journal of engineering mechanics, 127(5), 421-431.

Maccarini H, Vasconcelos G, Rodrigues H, Ortega J and Lourenço PB (2018) Out-of-plane behavior of stone masonry walls: Experimental and numerical analysis. Construction and Building Materials, 179, 430-452.

Lourenço, P. J. B. B. (1996) Computational strategies for masonry structures. Ph.D. dissertation.Delft (The Netherlands): Delft University of Technology; 1996.

Magenes G and Calvi GM (1992) Cyclic behaviour ofbrick masonry walls. Earthquake Engineering, Tenth Conference 1992 Balkema. Rotterdam

Magenes G, Penna A and Galasco A (2010) A full-scale shaking table test on a two-storey stone masonry building. In *14th European Conference on Earthquake Engineering*.

Modena C, Valluzzi MR, da Porto F and Casarin F (2011) Structural aspects of the conservation of historic masonry constructions in seismic areas: remedial measures and emergency actions. *International Journal of Architectural Heritage*, *5*(4-5), 539-558.

Mendes N (2012) Seismic assessment of ancient masonry buildings: shaking table tests and numerical analysis. Ph.D. dissertation, University of Minho: Portugal.

Mendes N, Lourenço PB and Campos-Costa A (2014) Shaking table testing of an existing masonry building: assessment and improvement of the seismic performance. *Earthquake engineering & structural dynamics*, *43*(2), 247-266.

Moreira S, Ramos LF, Oliveira DV and Lourenço PB (2014) Experimental behavior of masonry wall-to-timber elements connections strengthened with injection anchors. *Engineering Structures*, *81*, 98-109.

Mohammed A and Hughes TG (2011). Prototype and model masonry behaviour under different loading conditions. Materials and structures, 44(1), 53-65.

Mouzakis C, Adami CE, Karapitta L and Vintzileou E (2018) Seismic behaviour of timber-laced stone masonry buildings before and after interventions: shaking table tests on a two-storey masonry model. *Bulletin of Earthquake Engineering*, *16*(2), 803-829.

Okail HO, Shing PB, McGinley WM, Klingner RE, Jo S and McLean DI (2011) Shaking-table tests of a full-scale single-story masonry veneer wood-frame structure. *Earthquake engineering & structural dynamics*, *40*(5), 509-530.

Pande GN, Liang JX and Middleton J (1989) Equivalent elastic moduli for brick masonry. Computers and Geotechnics, 8(3), 243-265.

Paquette J and Bruneau M (2003). Pseudo-dynamic testing of unreinforced masonry building with flexible diaphragm. *Journal of structural engineering*, *129*(6), 708-716.

Paquette J, Bruneau M and Brzev S (2004) Seismic testing of repaired unreinforced masonry building having flexible diaphragm. *Journal of Structural Engineering*, *130*(10), 1487-1496.

Petry S and Beyer K (2014a) Scaling unreinforced masonry for reduced-scale seismic testing. *Bulletin of earthquake engineering*, *12*(6), 2557-2581.

Petry S and Beyer K (2014b). Influence of boundary conditions and size effect on the drift capacity of URM walls. *Engineering structures*, 65, 76-88.

PIET 70 (1971) Obras de fábrica. Prescripciones del Instituto Eduardo Torroja. Consejo Superior de Investigaciones Científicas Madrid: Instituto Eduardo Torroja (in Spanish).

Rafi MM, Lodi SH, Qazi SA, Kumar A and Verjee F (2018) Seismic response of reduced scale stone masonry building. *Proceedings of the Institution of Civil Engineers-Structures and Buildings*, *171*(7), 528-541.

Russo S (2013) Testing and modelling of dynamic out-of-plane behaviour of the historic masonry façade of Palazzo Ducale in Venice, Italy. *Engineering Structures*, 46, 130-139.

Senaldi IE, Guerrini G, Comini P, Graziotti F, Penna A, Beyer K and Magenes G (2020) Experimental seismic performance of a half-scale stone masonry building aggregate. *Bulletin of Earthquake Engineering*, *18*(2), 609-643.

Senthivel R and Lourenço PB (2009). Finite element modelling of deformation characteristics of historical stone masonry shear walls. Engineering structures, 31(9), 1930-1943.

Solarino F, Oliveira DV and Giresini L (2019) Wall-to-horizontal diaphragm connections in historical buildings: A state-of-the-art review. Engineering Structures, 199, 109559.

Stavridis A, Ahmadi F, Mavros M, Shing PB, Klingner RE and McLean D (2016). Shake-table tests of a full-scale three-story reinforced masonry shear wall structure. Journal of Structural Engineering, 142(10), 04016074.

Sweeney SC, Horney MA and Orton SL (2004) Tri-directional seismic analysis of an unreinforced masonry building with flexible diaphragms.

Sweeney SC, Horney MA and Orton SL (2005) *Seismic response of a half-scale masonry building with flexible diaphragms*. ENGINEER RESEARCH AND DEVELOPMENT CENTER CHAMPAIGN IL CONSTRUCTION ENGINEERING RESEARCH LAB.

Szirtes T (2007) *Applied dimensional analysis and modeling*. Butterworth-Heinemann.

Tomazevic M (1999) Earthquake-resistant design of masonry buildings (Vol. 1). Imperial College Press.

Tomazevic M and Velechovsky T (1992) Some aspects of testing small-scale masonry building models on simple earthquake simulators. *Earthquake engineering & structural dynamics*, *21*(11), 945-963.

Tomaževič M, Klemenc I and Weiss P (2009). Seismic upgrading of old masonry buildings by seismic isolation and CFRP laminates: a shaking-table study of reduced scale models. *Bulletin of earthquake engineering*, *7*(1), 293-321.

Valluzzi MR, Da Porto F and Modena C (2004). Behavior and modeling of strengthened three-leaf stone masonry walls. *Materials and structures*, 37(3), 184-192.

Van Eldere H, Ramos LF, Verstrynge E, Shetty N, Van Balen K, Barroso CE and Oliveira DV (2019). The application of sonic testing on double-leaf historical

Portuguese masonry to obtain morphology and mechanical properties. In Structural Analysis of Historical Constructions (pp. 661-668). Springer, Cham.

Vintzileou E, Mouzakis C, Adami CE and Karapitta L (2015) Seismic behavior of three-leaf stone masonry buildings before and after interventions: Shaking table tests on a two-storey masonry model. *Bulletin of Earthquake Engineering*, *13*(10), 3107-3133.

Vintzileou E (2008). Effect of timber ties on the behavior of historic masonry. *Journal of structural engineering*, *134*(6), 961-972.

Weise K, Gautam D and Rodrigues H (2018) Response and rehabilitation of historic monuments after the Gorkha earthquake. In *Impacts and insights of the Gorkha Earthquake* (pp. 65-94). Elsevier.

Žarnić R, Gostič S, Crewe AJ, & Taylor CA (2001) Shaking table tests of 1: 4 reduced-scale models of masonry infilled reinforced concrete frame buildings. *Earthquake engineering & structural dynamics*, *30*(6), 819-834.

Zonta D, Zanardo G and Modena C (2001) Experimental evaluation of the ductility of a reduced-scale reinforced masonry building. *Materials and Structures*, *34*(10), 636-644.

Tables

Table 1 – Comparison of similitude laws.

parameters	symbol	dimension*a*	Cauchy	Cauchy-Froude	Senaldi (2020)	Krawinkler (1979)
Geometric parameters						
length	L	L	λ	λ	λ	λ
area	A	L^2	λ^2	λ^2	λ^2	λ^2
volume	V	L^3	λ^3	λ^3	λ^3	λ^3
moment of inertia	*I*	L^4	λ^4	λ^4	λ^4	λ^4
Material parameters						
density	ρ	FL^{-3}	1	λ^{-1}	1	*b
modulus of elasticity	*E*	FL^{-2}	1	1	λ	λ
stress	σ	FL^{-2}	1	1	λ	λ
strain	ε	1	1	1	1	1
Poisson's ratio	ν	1	1	1	1	N/A
Dynamic parameters						
displacement	d	L	λ	λ	λ	λ
velocity	v	T^{-1}	1	$\lambda^{1/2}$	$\lambda^{1/2}$	$\lambda^{1/2}$
acceleration	a	T^{-2}	λ^{-1}	1	1	1
time	t	T	λ	$\lambda^{1/2}$	$\lambda^{1/2}$	$\lambda^{1/2}$
frequency	f	T^{-1}	λ^{-1}	$\lambda^{-1/2}$	$\lambda^{-1/2}$	$\lambda^{-1/2}$
mass	m	F	λ^3	λ^2	λ^3	N/A
force	F	F	λ^2	λ^2	λ^3	λ^3

NB) *a* F=force, L=length, T=time

b Detailed discussion is found in the publication of Krawinkler (1979).

Table 2 – Adopted material properties of the two-storey building.

	stone masonry	**timber**
Density (kg/m3)	2,000	420
Compressive strength (MPa)	4	20
Modulus of elasticity (MPa)	350	10,000
Tensile strength (MPa)	0.1	20
Tensile fracture energy (N/m)	30	-
Poisson ratio (-)	0.2	0.3

Table 3 – Eigenvalue analysis of the two-storey building in the X direction.

X (Hz)	prototype	mock-up CF	mock-up C	Y (Hz)	prototype	mock-up CF	mock-up C
1st	2.55	2.55	2.54	**1st**	4.11	4.12	4.11
2nd	5.59	5.63	5.58	**2nd**	8.73	8.78	8.76
participation factors (PF) (%)	**prototype**	**mock-up CF**	**mock-up C**	**PF (%)**	**prototype**	**mock-up CF**	**mock-up C**
1st	56.0	55.9	55.8	**1st**	69.5	69.4	69.5
2nd	13.9	13.0	14.1	**2nd**	4.31	4.30	2.50

Table 4 – Eigenvalue comparison of the two-storey building with the real structure.

	experiment (Hz)	**FEM (Hz)**	**error (%)**	**PF (%)**
X	6.05	6.15	-1.73	12.4
Y	4.21	4.18	0.69	55.6

Table 5 – Adopted material properties of the four-storey building.

	stone masonry (transverse walls)	**stone masonry (longitudinal walls)**	**timber beams**	**MDF panels**
Density (kg/m3)	2,160	2,160	580	580
Compressive strength (MPa)	2	6	20	20
Modulus of elasticity (MPa)	640	3,300	12,000	160
Tensile strength (MPa)	0.1	0.1	20	20
Tensile fracture energy (N/m)	30	30	-	-
Poisson ratio (-)	0.2	0.2	0.3	0.3

Table 6 – Eigenvalue comparison of the four-storey building.

X (Hz)	prototype	mock-up CF	mock-up C	experiment	Y (Hz)	prototype	mock-up CF	mock-up C	experiment
1st	1.73	1.77	1.73	1.64	**1st**	4.32	4.19	4.26	4.03
2nd	5.06	5.20	5.05	5.42	**2nd**	5.27	5.27	5.19	4.77
PF (%)	**prototype**	**mock-up CF**	**mock-up C**	**experiment**	**PF (%)**	**prototype**	**mock-up CF**	**mock-up C**	**experiment**
1st	70.5	70.4	70.1	-	**1st**	31.4	29.8	31.1	-
2nd	7.08	6.81	5.14	-	**2nd**	0.16	0.15	0.16	-

Figures

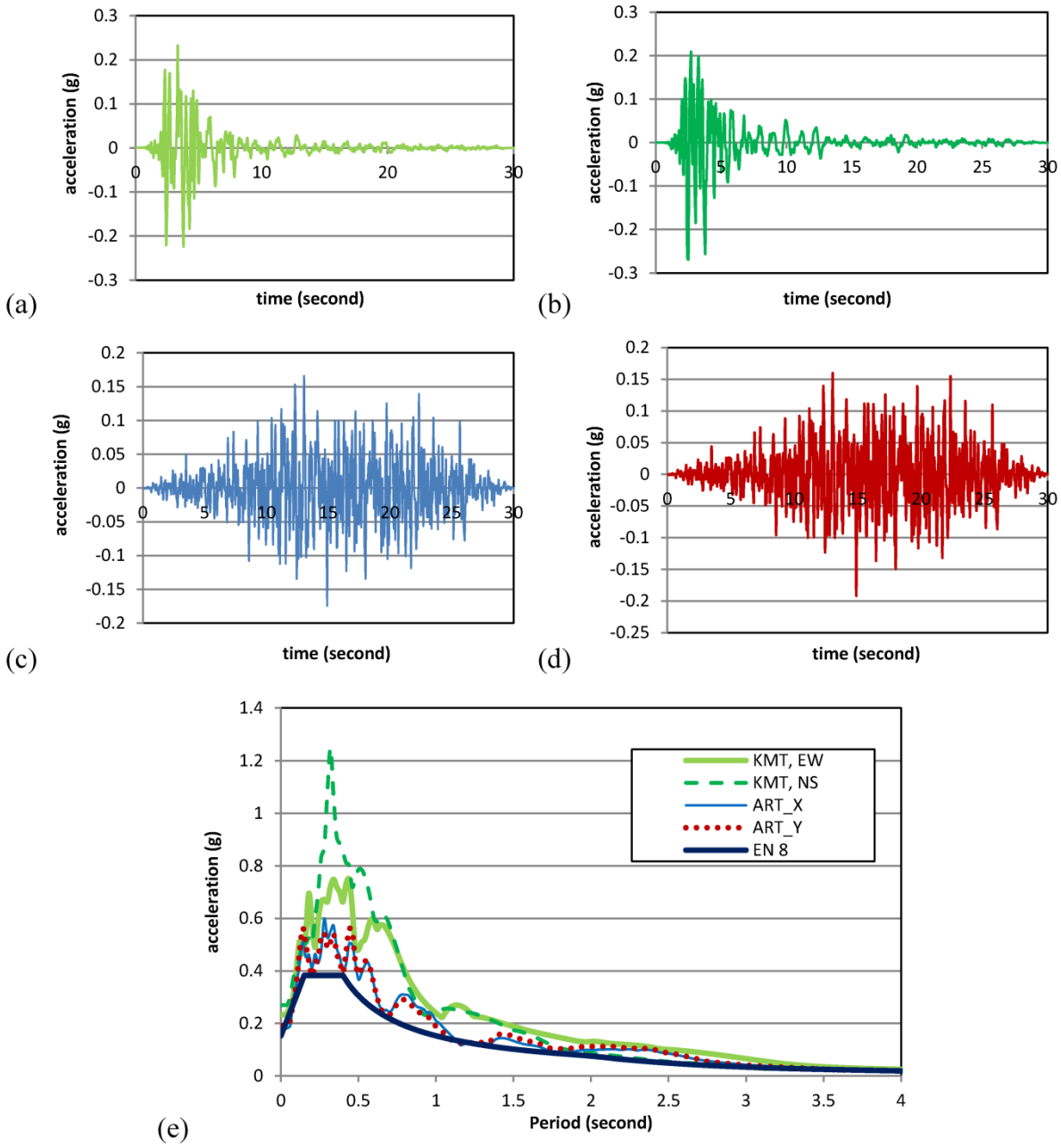

Figure 1 – adopted accelerograms: acceleration time-history of Kalamata earthquake in the EW direction (a), in the NS direction, acceleration time-history of the artificial accelerogram in the X direction (c), in the Y direction (d) and (e) response spectra.

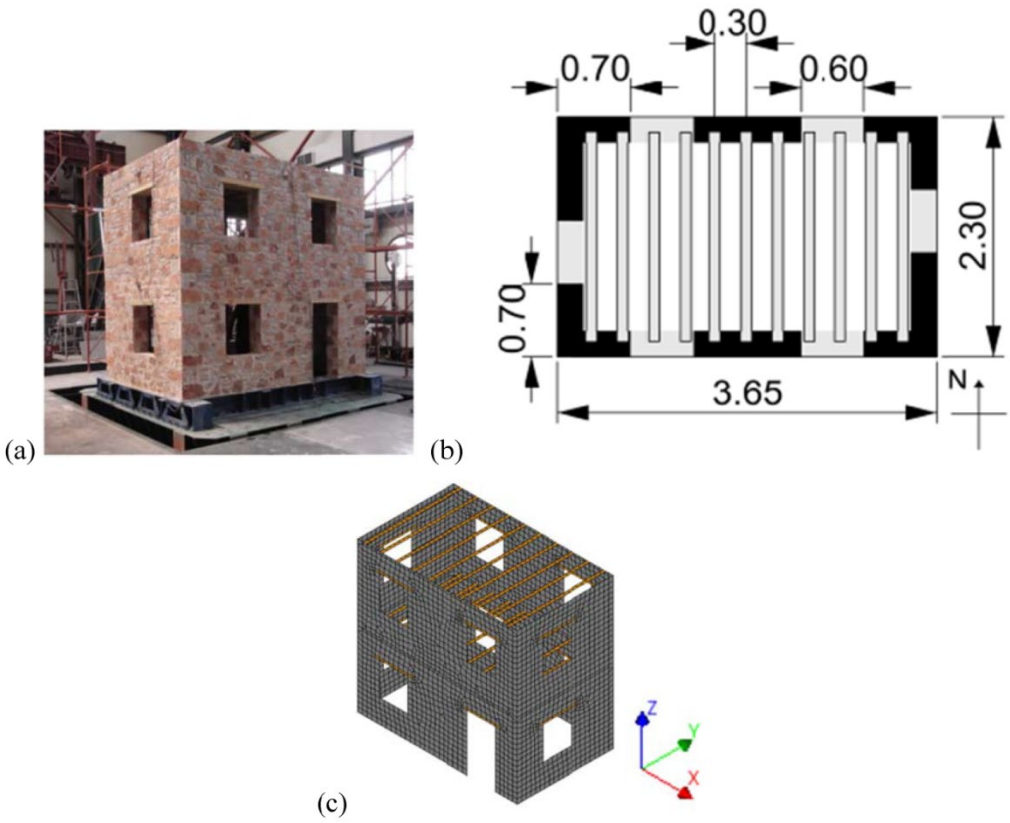

Figure 2 – Two storey building: (a) the tested prototype, (b) plan (unit: m) and (c) FE model (a from Vintzileou et al. 2015).

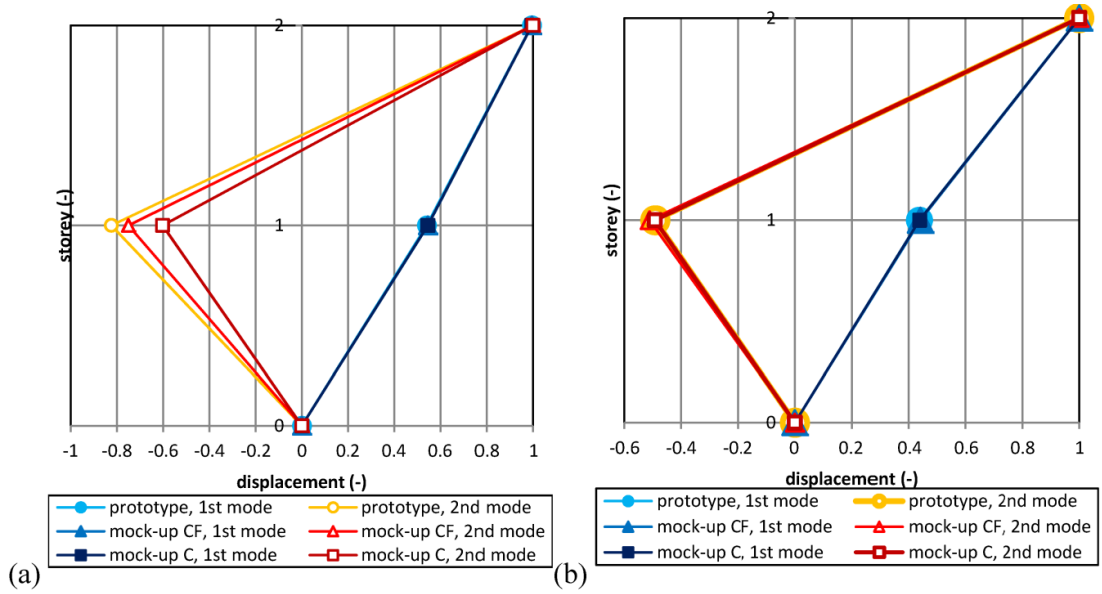

Figure 3 – Mode shapes of the two-storey building: (a) the east wall in the X direction and (b) the north wall in the Y direction.

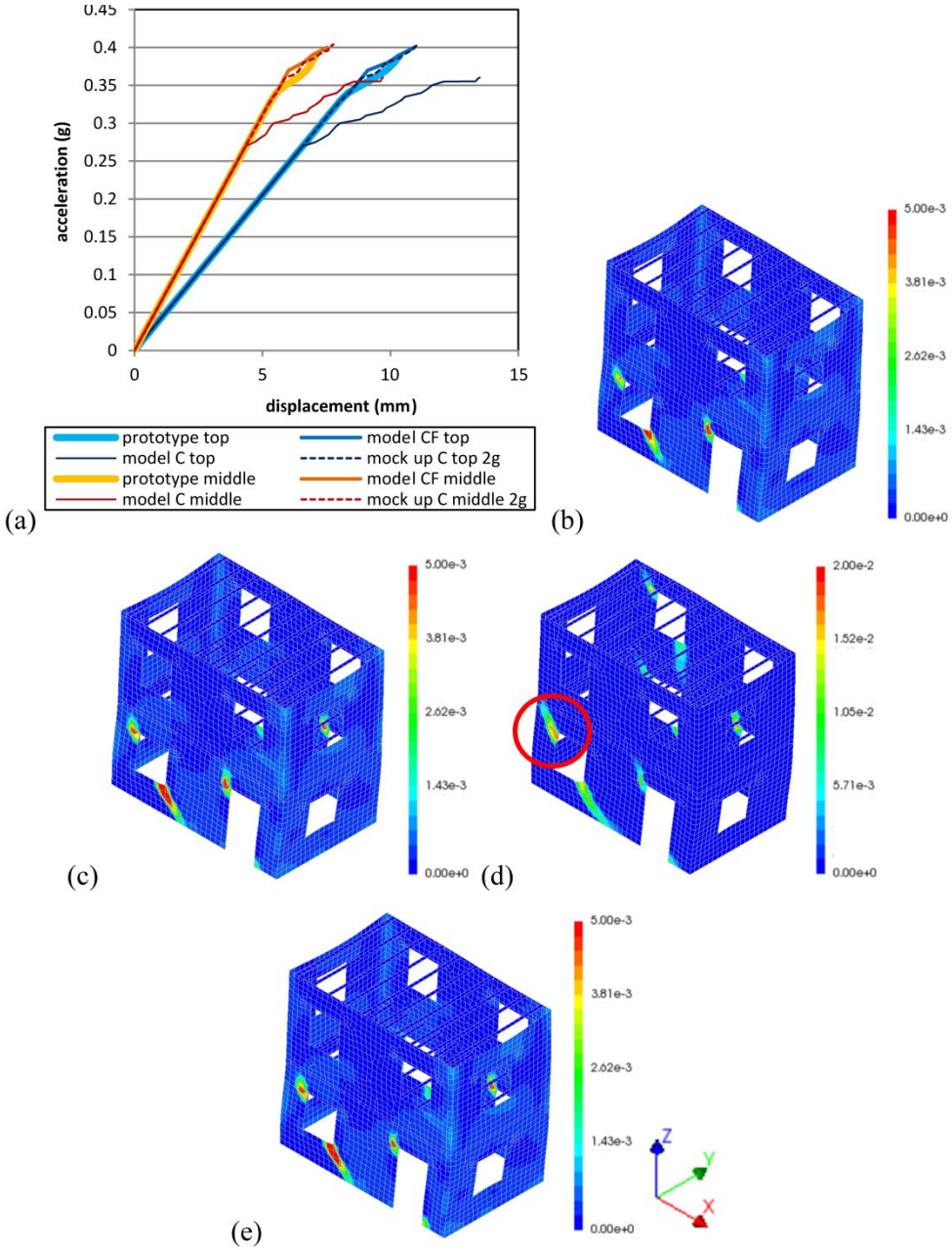

Figure 4 – Pushover analysis of the two-storey building in the positive X direction: (a) base acceleration-displacement relations, principal positive strain contours close to the collapse of prototype (b), of mock-up CF (c), of mock-up C (d) and mock-up eC (e).

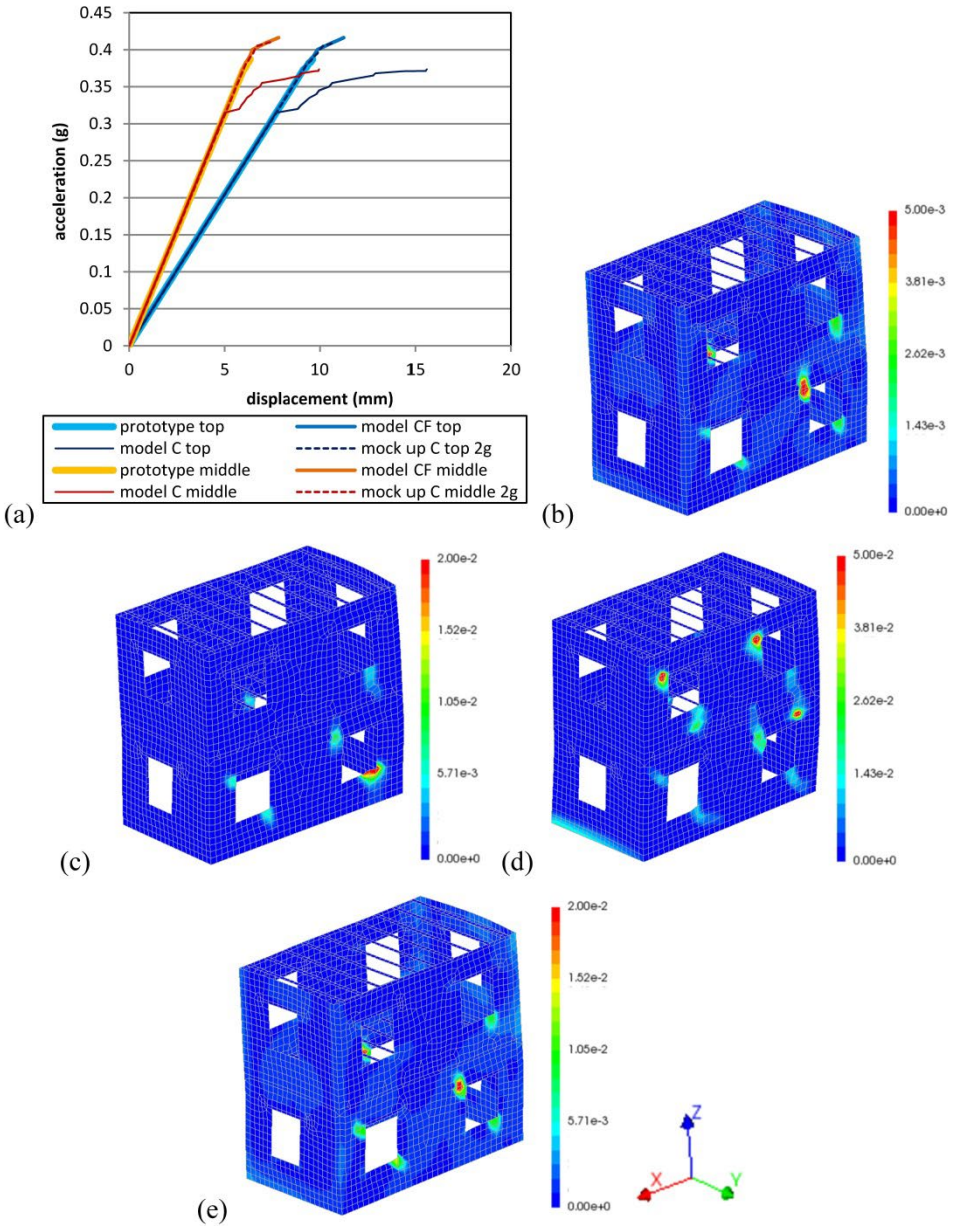

Figure 5 – Pushover analysis of the two-storey building in the negative X direction: (a) base acceleration-displacement relations, principal positive strain contours close to the collapse of prototype (b), of mock-up CF (c), of mock-up C (d) and mock-up eC (e).

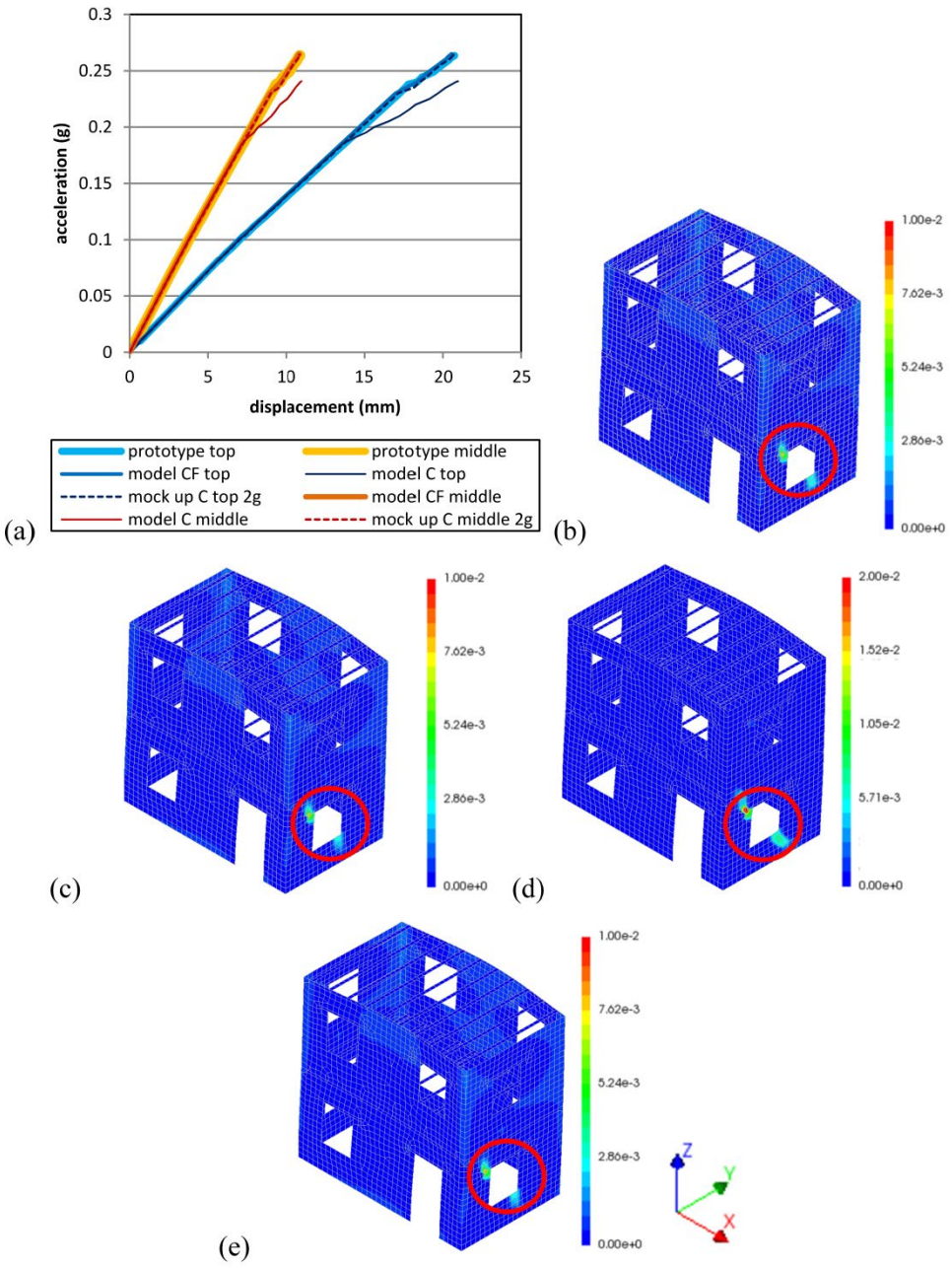

Figure 6 – Pushover analysis of the two-storey building in the positive Y direction: (a) base acceleration-displacement relations, principal positive strain contours close to the collapse of prototype (b), of mock-up CF (c), of mock-up C (d) and mock-up eC (e).

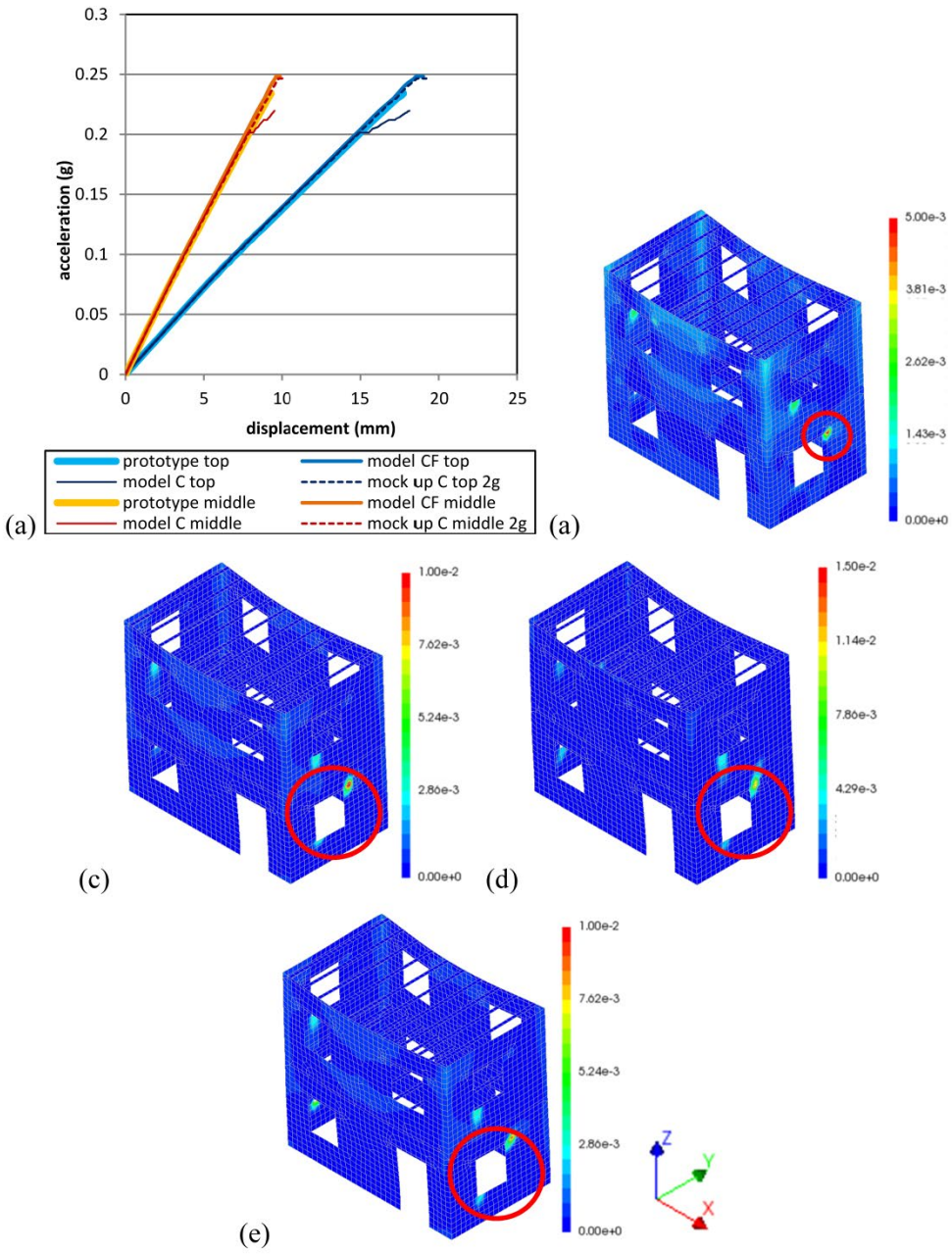

Figure 7 – Pushover analysis of the two-storey building in the positive Y direction: (a) base acceleration-displacement relations, principal positive strain contours close to the collapse of prototype (b), of mock-up CF (c), of mock-up C (d) and mock-up eC (e).

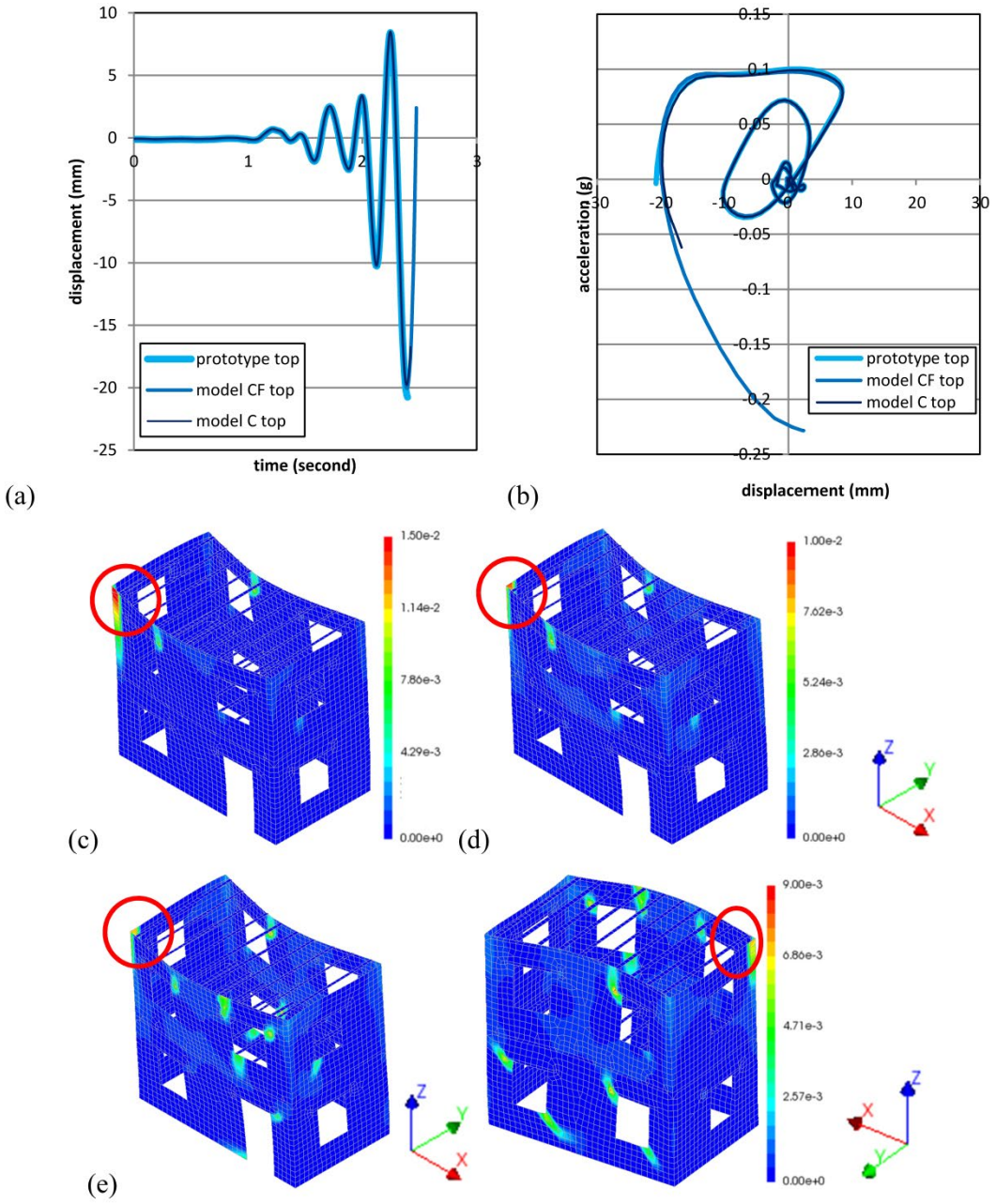

Figure 8 – Nonlinear dynamic analysis of a two-storey building under the Kalamata earthquake in the Y direction: (a) time history of the top of the structure, (b) base acceleration-displacement relations principal positive strain contours of the prototype at 2.40 seconds (c), of the mock-up CF at 2.39 seconds (d) and of the mock-up C at 2.39 seconds (e).

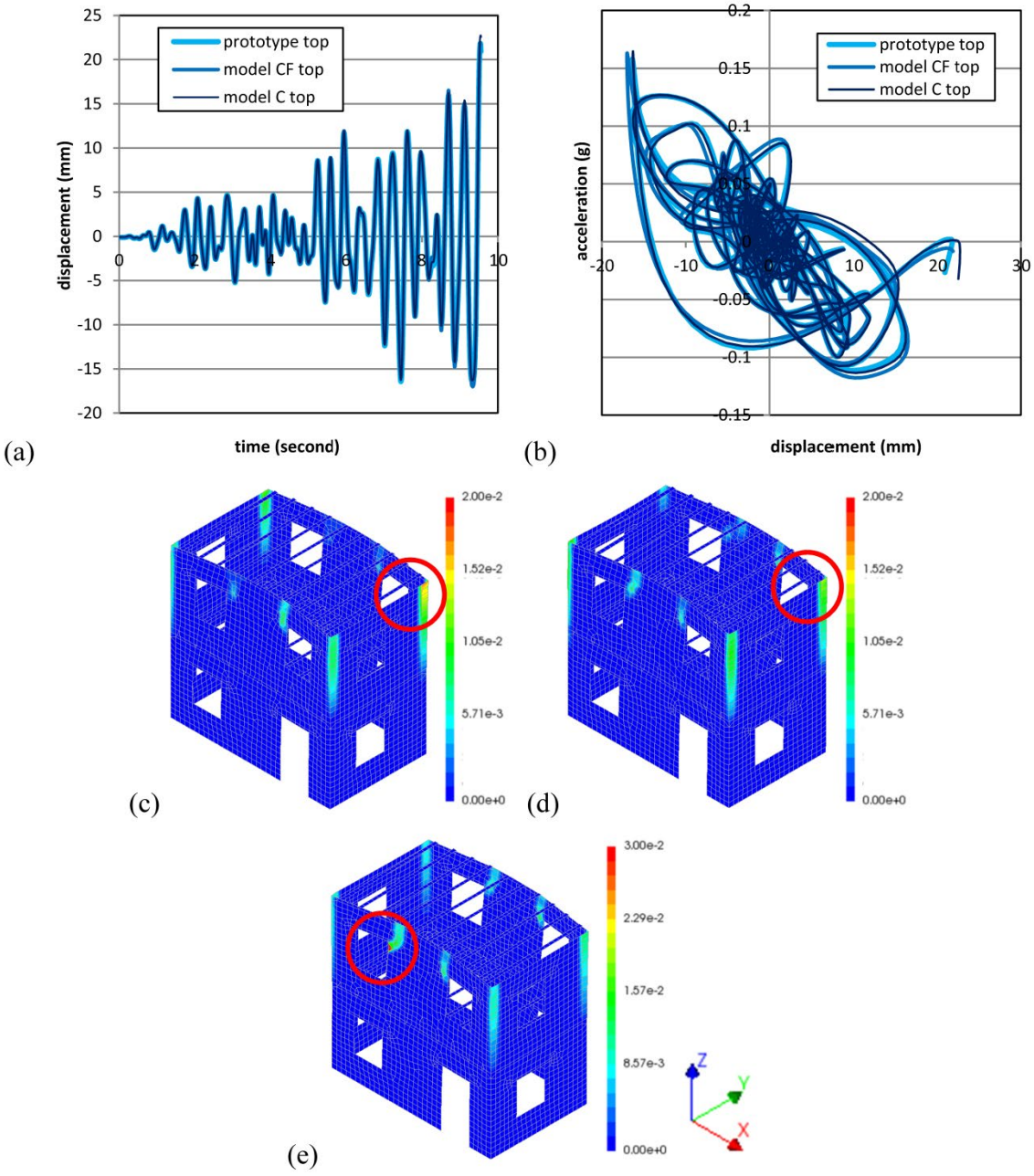

Figure 9 – Nonlinear dynamic analysis of a two-storey building under the artificial earthquake in the Y direction: (a) time history of the top of the structure, (b) base acceleration-displacement relations, principal positive strain contours of the prototype at 9.54 seconds (c), of the mock-up CF at 9.53 seconds (d) and of the mock-up C at 9.54 seconds (e).

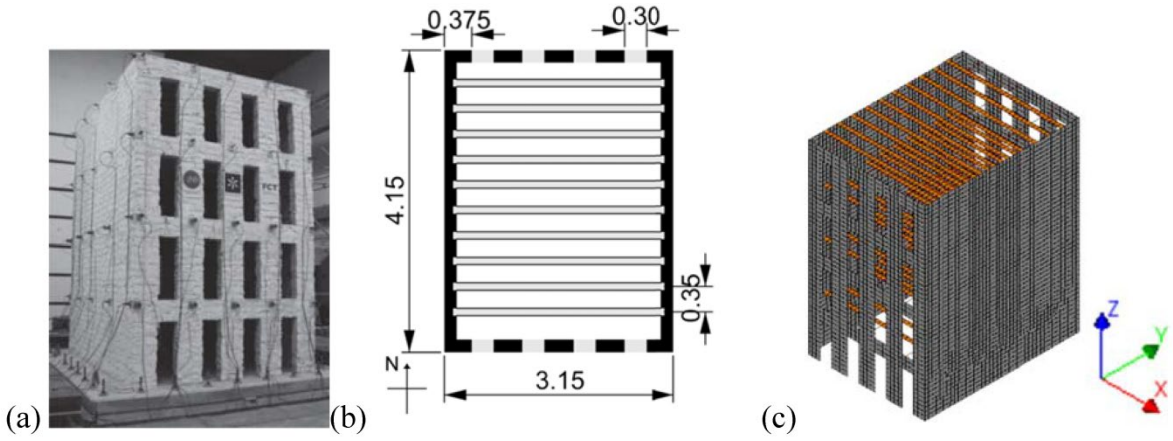

Figure 10 – Four storey building: (a) the tested prototype (b) plan (unit: m) and (c) FE model (a from Mendes et al. 2014).

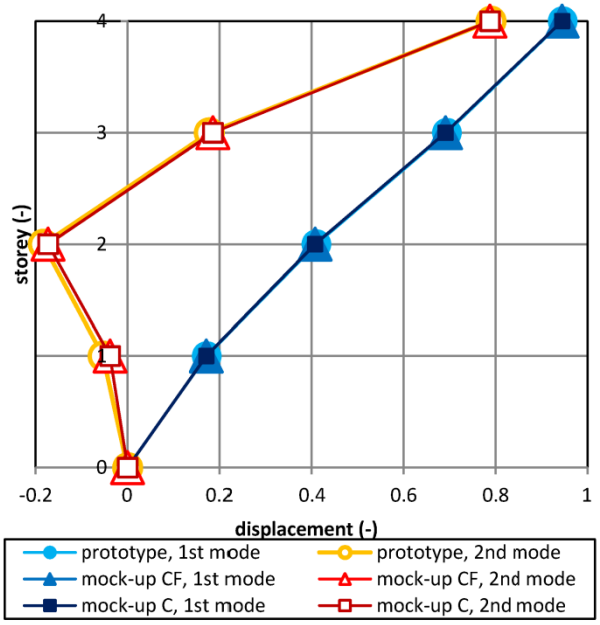

Figure 11 – Eigenvalue shapes of the longitudinal wall of the four-storey building in the X direction.

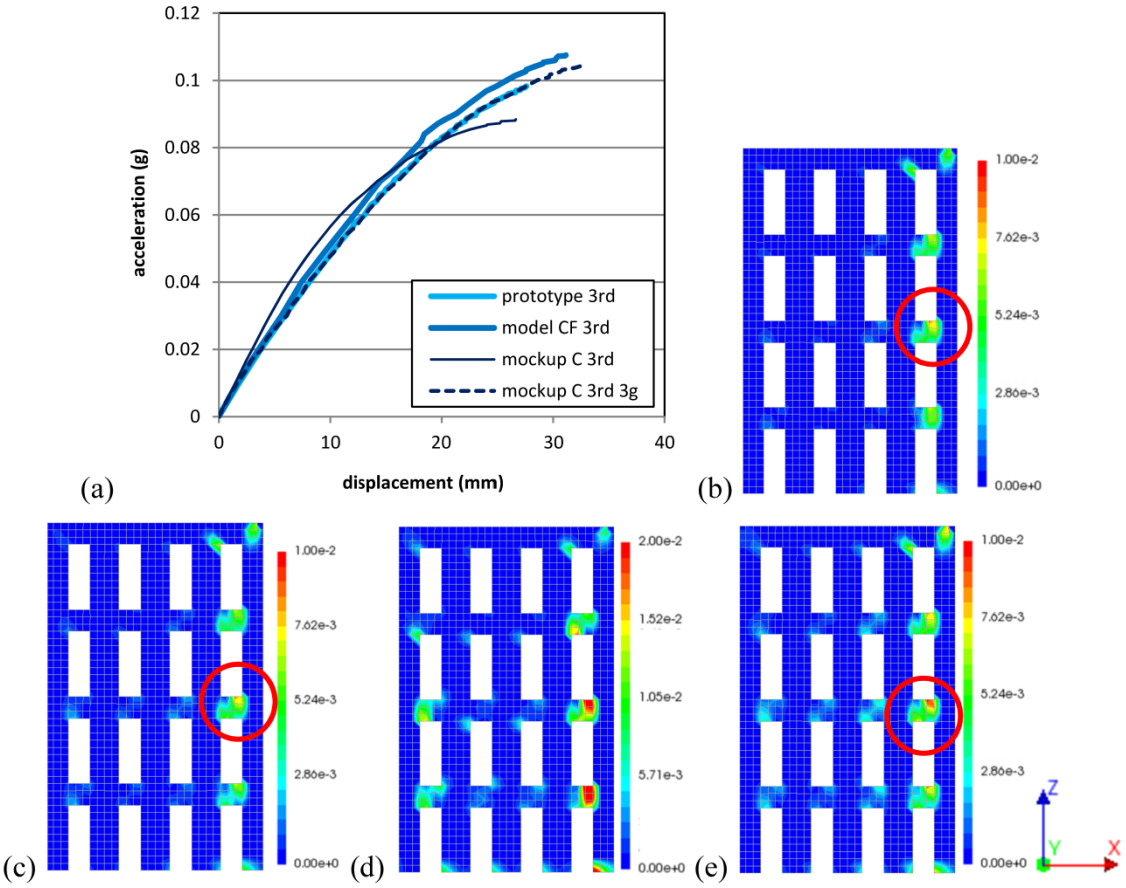

Figure 12 – Pushover analysis of the four-storey building in the X direction: (a) base acceleration-displacement relations, principal positive strain contours of the south elevation close to the collapse of prototype (b), of mock-up CF (c), of mock-up C (d) and mock-up eC (e).

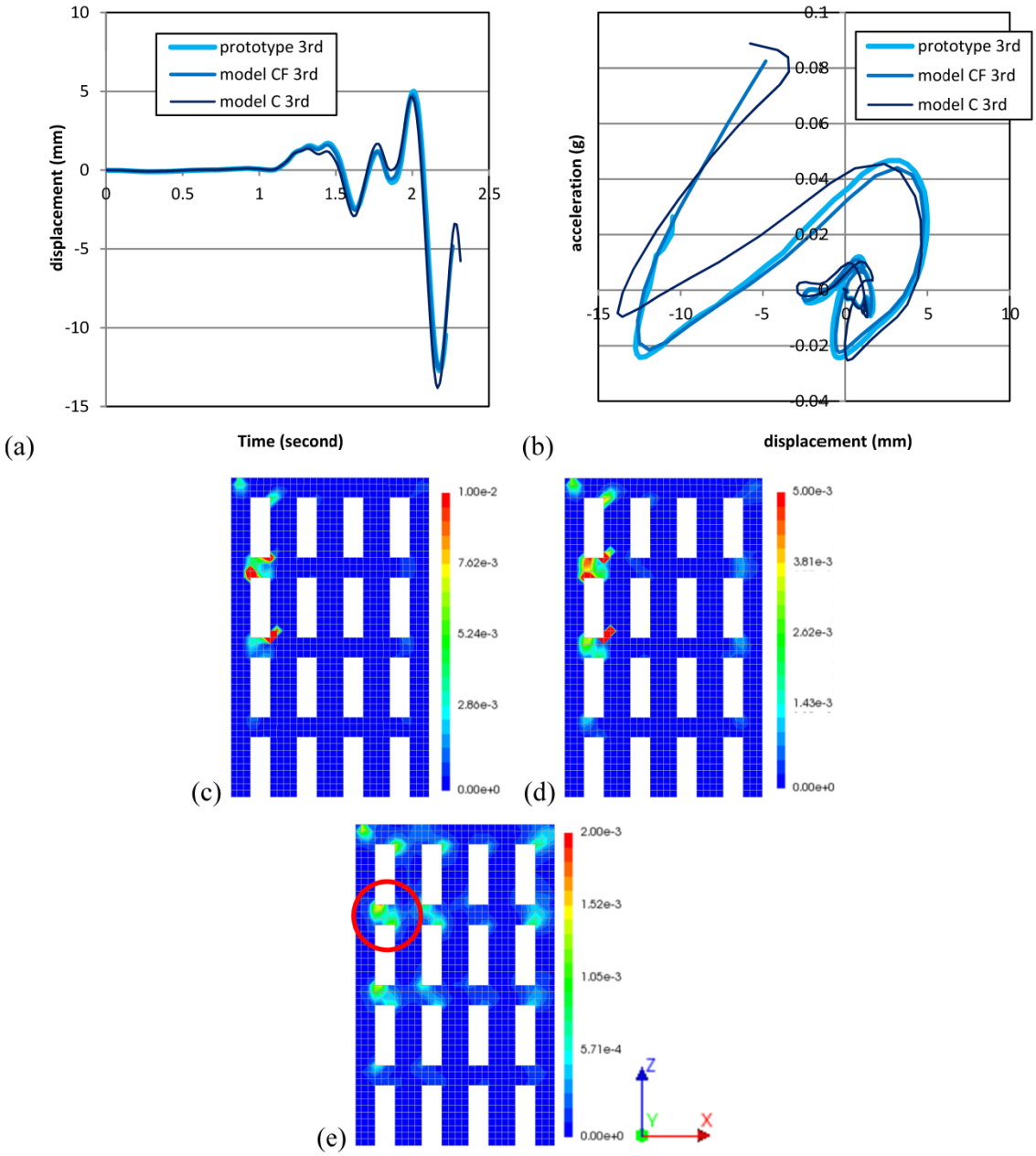

Figure 13– Nonlinear dynamic analysis of the four-storey building under the Kalamata earthquake in the X direction: (a) time history of the top of the structure and (b) base acceleration-displacement relations, principal positive strain contours of the south elevation of the prototype at 2.18 seconds (c), of the mock-up CF at 2.16 seconds (d) and of the mock-up C at 2.16 seconds (e).

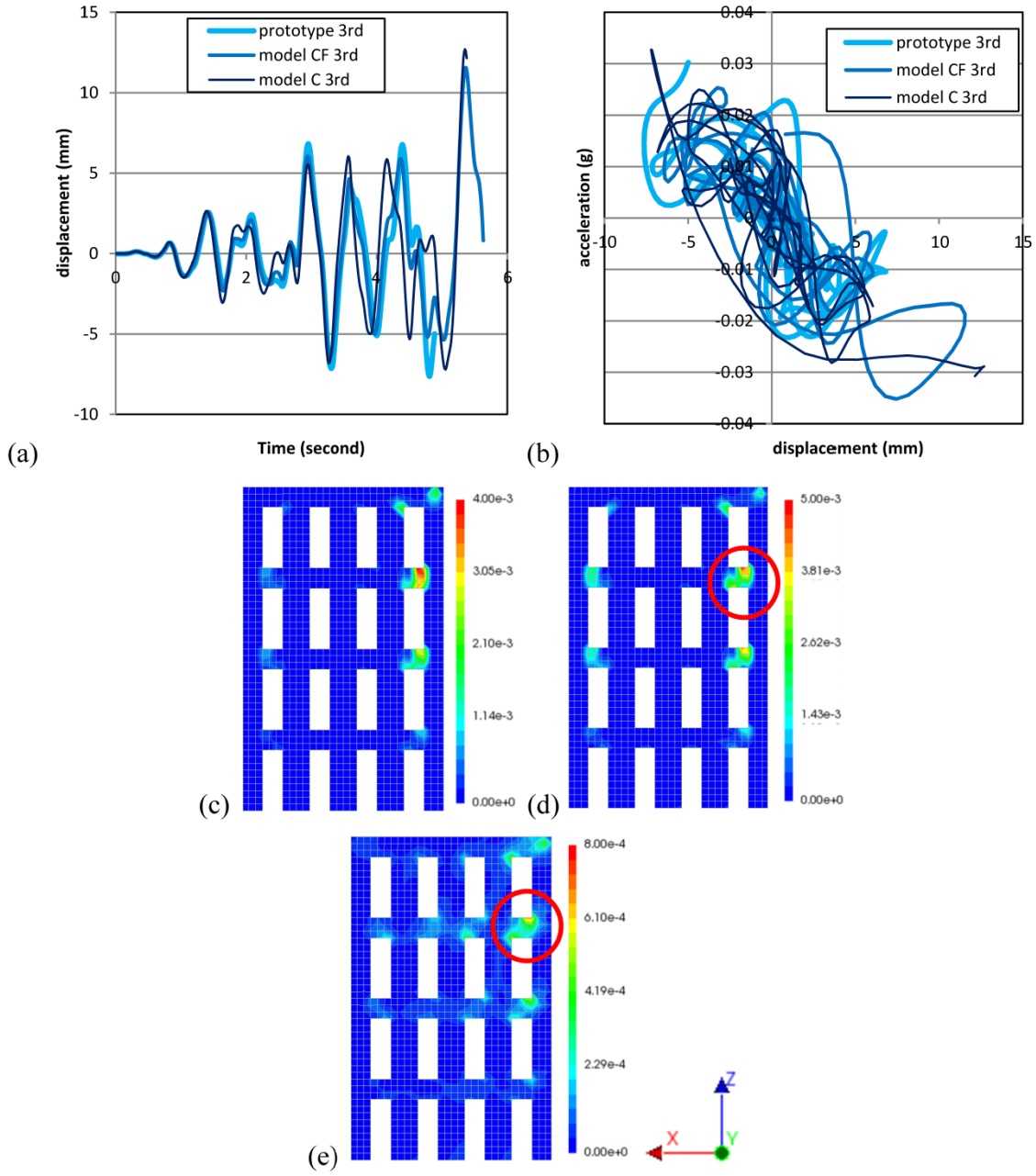

Figure 14 – Nonlinear dynamic analysis of a two-storey building under the artificial earthquake in the X direction: (a) time history of the top of the structure, (b) base acceleration-displacement relations principal positive strain contours of the north elevation of the prototype at 4.81 seconds (c), of the mock-up CF at 4.78 seconds (d) and of the mock-up C at 4.50 seconds (e).

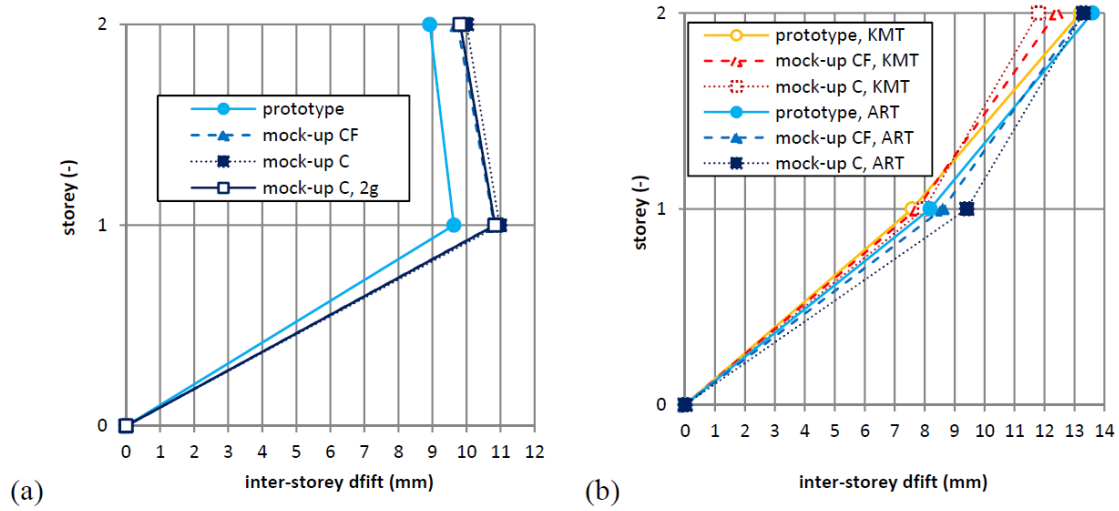

Figure 15 – The inter-storey drift of the two-storey building in the Y direction: (a) at the last step of pushover analysis in the positive direction, (b) at the last local peak of NDA.

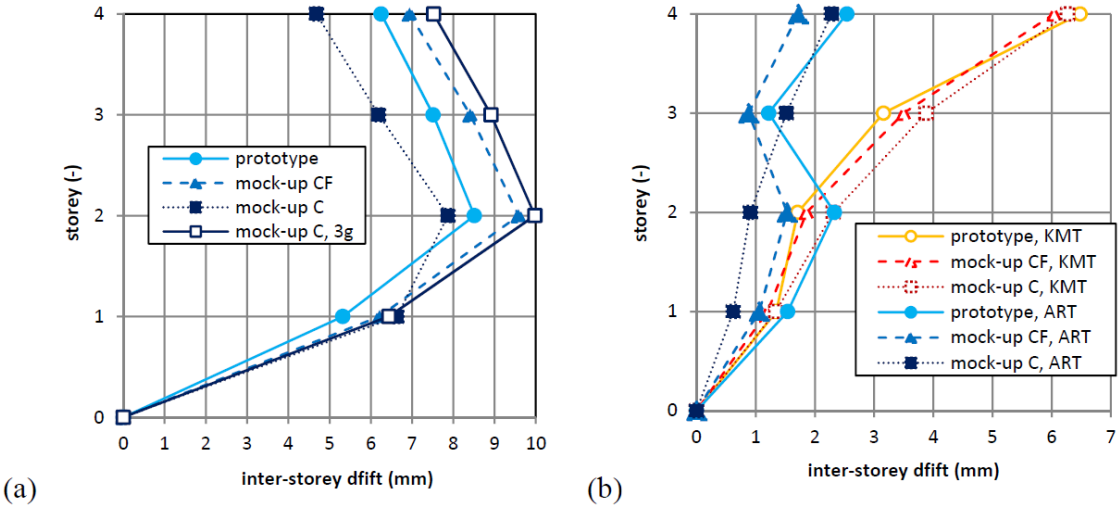

Figure 16 - The inter-storey drift of the four-storey building in the X direction: (a) at the last step of pushover analysis, (b) at the last local peak of NDA.

Figure captions

Figure 1 – adopted accelerograms: acceleration time-history of Kalamata earthquake in the EW direction (a), in the NS direction, acceleration time-history of the artificial accelerogram in the X direction (c), in the Y direction (d) and (e) response spectra.

Figure 2 – Two storey building: (a) the tested prototype, (b) plan (unit: m) and (c) FE model (a from Vintzileou et al. 2015).

Figure 3 – Mode shapes of the two-storey building: (a) the east wall in the X direction and (b) the north wall in the Y direction.

Figure 4 – Pushover analysis of the two-storey building in the positive X direction: (a) base acceleration-displacement relations, principal positive strain contours close to the collapse of prototype (b), of mock-up CF (c), of mock-up C (d) and mock-up eC (e).

Figure 5 – Pushover analysis of the two-storey building in the negative X direction: (a) base acceleration-displacement relations, principal positive strain contours close to the collapse of prototype (b), of mock-up CF (c), of mock-up C (d) and mock-up eC (e).

Figure 6 – Pushover analysis of the two-storey building in the positive Y direction: (a) base acceleration-displacement relations, principal positive strain contours close to the collapse of prototype (b), of mock-up CF (c), of mock-up C (d) and mock-up eC (e).

Figure 7 – Pushover analysis of the two-storey building in the positive Y direction: (a) base acceleration-displacement relations, principal positive strain contours close to the collapse of prototype (b), of mock-up CF (c), of mock-up C (d) and mock-up eC (e).

Figure 8 – Nonlinear dynamic analysis of a two-storey building under the Kalamata earthquake in the Y direction: (a) time history of the top of the structure, (b) base acceleration-displacement relations principal positive strain contours of the prototype at 2.40 seconds (c), of the mock-up CF at 2.39 seconds (d) and of the mock-up C at 2.39 seconds (e).

Figure 9 – Nonlinear dynamic analysis of a two-storey building under the artificial earthquake in the Y direction: (a) time history of the top of the structure, (b) base acceleration-displacement relations, principal positive strain contours of the prototype at

9.54 seconds (c), of the mock-up CF at 9.53 seconds (d) and of the mock-up C at 9.54 seconds (e).

Figure 10 – Four storey building: (a) the tested prototype (b) plan (unit: m) and (c) FE model (a from Mendes et al. 2014).

Figure 11 – Eigenvalue shapes of the longitudinal wall of the four-storey building in the X direction.

Figure 12 – Pushover analysis of the four-storey building in the X direction: (a) base acceleration-displacement relations, principal positive strain contours of the south elevation close to the collapse of prototype (b), of mock-up CF (c), of mock-up C (d) and mock-up eC (e).

Figure 13– Nonlinear dynamic analysis of the four-storey building under the Kalamata earthquake in the X direction: (a) time history of the top of the structure and (b) base acceleration-displacement relations, principal positive strain contours of the south elevation of the prototype at 2.18 seconds (c), of the mock-up CF at 2.16 seconds (d) and of the mock-up C at 2.16 seconds (e).

Figure 14 – Nonlinear dynamic analysis of a two-storey building under the artificial earthquake in the X direction: (a) time history of the top of the structure, (b) base acceleration-displacement relations principal positive strain contours of the north elevation of the prototype at 4.81 seconds (c), of the mock-up CF at 4.78 seconds (d) and of the mock-up C at 4.50 seconds (e).

Figure 15 – The inter-storey drift of the two-storey building in the Y direction: (a) at the last step of pushover analysis in the positive direction, (b) at the last local peak of NDA.

Figure 16 - The inter-storey drift of the four-storey building in the X direction: (a) at the last step of pushover analysis, (b) at the last local peak of NDA.